VILNIUS TECH
Vilnius Gediminas Technical University

Journal of Environmental Engineering and Landscape Management
ISSN 1648–6897 / eISSN 1822-4199
2022 Volume 30 Issue 1: 56–65
https://doi.org/10.3846/jeelm.2022.16251

SYNTHESIS OF FEOOH AND FEOOH@ZNO BY HYDROTHERMAL METHOD AND THE ADSORPTION OF S^{2-} IN WASTEWATER

Baocai GE, Fen LI*, Fanzhu MENG, Ying YANG, Cailian YU

School of Materials Science and Chemical Engineering, Harbin University of Science and Technology, 150040 Heilongjiang Province, Harbin, China

Received 24 February 2020; accepted 17 July 2021

Highlights

- A new desulfurizer FeOOH @ ZnO was prepared to remove S^{2-}. It has obvious effect on S^{2-} removal.
- FeOOH@ZnO has efficient desulfurization effect, and the adsorption capacity of S^{2-} can reach 87.5 $mg \cdot g^{-1}$.
- Through characterization analysis, iron is mainly present as Fe^{3+}, while oxygen in Fe = O is replaced by sulfur, and ferrous precipitates appear.

Abstract. FeOOH and FeOOH@ZnO were prepared by hydrothermal synthesis, and their structures and adsorption properties toward S^{2-} were studied. The results showed that too high hydrothermal temperature was not conducive to the adsorption of S^{2-}. However, using sodium dodecyl sulfate (SDS) for FeOOH preparation and adding nanometer ZnO (FeOOH@ZnO) could significantly improve the adsorption of S^{2-} by FeOOH, and adsorption removal rate was close to 90.0% and adsorption amount was 87.5 $mg \cdot g^{-1}$. The structural analysis showed that the modification of FeOOH by SDS and the addition of nano-ZnO resulted in the reduction in size of the FeOOH particles, forming amorphous inclusion structure with ZnO present inside and FeOOH outside. The specific surface area of FeOOH@ZnO was found to be higher than that of FeOOH. Therefore, it is beneficial to the adsorption of S^{2-}. XPS fitting results showed that ferrous deposits appeared in the process of adsorption of S^{2-} by FeOOH@ZnO, and it was considered that the oxygen of Fe = O was replaced with sulfur.

Keywords: hydrothermal synthesis, adsorption of S^{2-}, FeOOH, FeOOH@ZnO.

Introduction

With the rapid development of industrial technology, the problem of environmental pollution has become progressively more serious. In particular, in industries closely related to life, such as refining, petrochemical, pharmaceutical, and tanning, a large amount of sulfur-containing wastewater is generated during the production process (Wei, 2003). Sulfide ions (S^{2-}) in wastewater can corrode metal materials, poison the human body, and release malodorous gases, posing serious hazards to the human health and environment (Liang et al., 2020; Liu et al., 2020; Zhang et al., 2018b). Gas extraction method (Zhou et al., 2019), biological method (Qian et al., 2019), and precipitation method (Liu et al., 2019) are traditional methods for removing S^{2-} from wastewater. However, the gas extraction method consumes extensively large amount of energy and is not suitable for the treatment of low-concentration sulfur-containing wastewater. Although the biological treatment process is simple and the operating cost is low, the concentration of sulfide in water is not easy to be too high, and the sulfate wastewater needs to be disposed of. The precipitation method uses Fe^{2+}, Cu^{2+}, Zn^{2+} ions, and S^{2-} present in the wastewater to form sulfide precipitate for the removal of S^{2-}. In recent years, some advanced wastewater treatment technologies have also been applied to study sulfide removal. For example, Chen constructed a coupled microbial fuel cell (MFC) system composed of nitrification and sulfide removal MFC and denitrification and sulfide removal MFC (Chen et al., 2019) that could simultaneously treat ammonia and sulfide in wastewater. Moreover, at the same time, sulfide is converted into elemental sulfur to realize resource recovery. Tang selected a mixed solution of manganese sulfate ($MnSO_4$) and

*Corresponding author. E-mail: *hgxylf@126.com*

sulfuric acid (H_2SO_4) as the electrolyte (Tang et al., 2018). Under electrochemical oxidation conditions, the removal efficiency of sulfides reached 95.07%. Du used aluminum oxide and white alkane $(AAO+CEO)_2$ nanotubes as anode catalysts to remove sulfides present in diesel (Du et al., 2018), achieving a removal rate of over 90%. Although the sulfide removal efficiency of the above-mentioned method is high, the investment and energy consumption are large, and currently, it is not suitable for industrial scale-up. Adsorption technology has a wide range of applications in the field of environmental pollution control due to its high efficiency (Liu et al., 2021); in particular, the development of some new adsorption materials has significantly improved the purification effect of pollutants. However, currently, there is no suitable adsorbent for the adsorption of S^{2-} present in sulfur-containing wastewater. Therefore, it is particularly important to explore low-cost and high-efficiency S^{2-} adsorption materials.

Iron(III) oxide-hydroxide (FeOOH) exists widely in nature, and can also be prepared in the laboratory by precipitation, hydrothermal synthesis, and sol–gel methods (Seabold et al., 2012; Liu et al., 2007; Kwong et al., 2016), due to its economic benefit and high reactivity. It has been widely used in environmental protection in recent years. For the adsorption and removal of pollutants from wastewater, Zhang prepared copper (Cu)-doped $FeOOH/C_3N_4$ composites as photo-Fenton catalysts (Zhang et al., 2018a), which could efficiently and quickly adsorb methylene blue over wide pH range. Xiao (Xiao et al., 2016) used graphene with iron oxyhydroxide to remove 2-chlorophenol, and the removal effect could reach 88%. Yang (Yang et al., 2017) developed biochar-loaded ferric hydroxide, which adsorbed hexavalent chromium, with an optimal removal rate of 96%. Jaiswal (Jaiswal et al., 2013) used chemical precipitation method to prepare α-FeOOH as catalyst for the adsorption of Cd(II), and achieved high removal effect. In terms of exhaust gas treatment, activated carbon-supported FeOOH developed by Lee (Lee et al., 2017) could effectively remove H_2S in exhaust gas. α-FeOOH nanoparticles (NPs) prepared by Gao could remove H_2S and COS at low temperature. Furthermore, Fu (Fu et al., 2007) studied the adsorption performance of iron materials on SO_2 and obtained good adsorption effects. At the same time, sulfur existed on the surface of the material as sulfate. Song (Song et al., 2018) prepared core–shell NPs using ferric chloride and sodium salicylate with carbonaceous shell and FeOOH as core. In the process of selective catalytic reduction of nitric oxide (NO), the removal rate of NO could reach 99.8%.

Thus, FeOOH has large specific surface area (SSA) as well as oxidizing properties of ferric iron, and it is considered to be an efficient material for adsorbing S^{2-} present in wastewater; however, significant research attempts in this area have not been reported till date. Moreover, zinc oxide has excellent thermal and chemical stability. It is a widely used gas fine desulfurizer in chemical production. It also has good adsorption effect on industrial waste gas containing sulfide; however, only a few studies are available on the adsorption of pollutants present in water. Therefore, FeOOH and FeOOH@ZnO were synthesized by hydrothermal method in this study. S^{2-} in the wastewater was used as the target pollutant. The preparation process conditions were optimized and the material structure was analyzed and characterized. This research can provide new adsorption material for the removal of sulfide in wastewater, and has certain practical value.

1. Experimental

1.1. Material preparation

A certain concentration of $FeCl_3$ and NaOH solution (0.4, 0.6, 0.7, 0.9, 1.0, 1.1, 1.25, 1.4, and 1.5 $mol \cdot L^{-1}$) was set, and $FeCl_3$ solution (20 mL) was taken in a conical flask. Sodium dodecyl sulfate (SDS) solution with certain concentration (0, 3, 4, 5, 6, and 7 $mmol \cdot L^{-1}$) was prepared, and then 20 mL of this solution was measured and slowly added to the above mentioned $FeCl_3$ solution. The different molar ratios of SDS: Fe were marked as 0.003:1, 0.004:1, 0.005:1, 0.006:1, and 0.007:1. The contents were vigorously stirred for 15 min to obtain homogeneous and uniform mixture. Then, NaOH solution with certain concentration was slowly added, the pH was adjusted to 12, the contents were stirred for 1 h, and finally the solution was transferred to the reaction kettle. The reaction kettle was placed in an oven and the contents were allowed to react at a certain hydrothermal temperature (100–130 °C) for 8.0 h. After the reaction, the precipitate in the kettle was filtered with suction, washed until the filtrate was neutral, and dried at 60 °C for 24 h to obtain FeOOH.

$FeCl_3$ solution with certain concentration was prepared, zinc ions or ZnO particles with a grain size of 20 nm were added according to the molar ratio of Fe to Zn (Fe:Zn) of 8.0:1, 4.0:1, and 2.5:1. Other preparation process parameters are the same as those for FeOOH, and FeOOH@ZnO was obtained.

1.2. Characterization

X-ray diffraction (XRD) analysis was carried out using a D8 Advance X-ray diffractometer (Bruker, Germany), equipped with Cu target and Kα radiation source. Tube voltage was 40 kV, tube current was 40 mA, scanning range was 5–80°, and scanning speed was 2°/min. Scanning electron microscopy (SEM) analysis was carried out using a scanning electron microscope (JSM-6380LV, JEOL Corporation of Japan), with an operating voltage of 20 kV. Transmission electron microscopy (TEM) analysis was carried out using a high-resolution transmission electron microscope (JEM-2100, Nippon Denshi Co., Ltd.). The sample was dispersed in absolute ethanol for 20–30 min, and then it was dispersed on carbon film-coated copper mesh, and then TEM analysis was carried out on the dried sample (the sample is scanned using magnetically protected transmission electron microscope lens). Fourier transform infrared (FTIR) spectroscopy analysis was carried out using an MR254 IR spectrometer (BoMEM, Canada),

with a scanning wavelength range of 4000–500 cm^{-1}. X-ray photoelectron spectroscopy (XPS) test was performed using American-made PHI5700 ESCA X-ray photoelectron spectrometer. The X-ray source used ALKα (hν = 1486.6 eV) rays, the target voltage was 13 KW, and the target power was 300 W. Raman spectra were recorded in the range from 100–1500 cm^{-1}, using a high resolution Raman spectrometer (Labram HR Evation, France) with He–Ne laser (633 nm). The SSA and pore structure analyses were performed using model 3H-2000PS1 SSA and porosity analyzer manufactured by China, Best Instrument Technology Co., Ltd., under liquid nitrogen atmosphere, and the pore size range was 3.5–5000 Å.

1.3. Detection of wastewater containing S^{2-}

Water sample with S^{2-} concentration of (50.0–150.0)± 0.5 $mg{\cdot}L^{-1}$, was prepared, and 100 mL of this sample was taken in a conical flask. FeOOH sample (0.1000±0.0005 g) was weighed, and added to the conical flask containing sulfur water. At the same time, a small amount of nitrogen was introduced to provide protecting environment above the liquid surface, and the conical flask was sealed with sealing film to prevent air from entering and causing large error. The conical flask was then placed on the shaker (under normal temperature and normal pressure), slowly shaken for 10–60 min, and then the contents were allowed to stand. Then, the supernatant was taken, and the residual sulfur ions in the water sample were measured by iodometric method (HJ/T60-2000). The same sample was measured three times in parallel, and experiment on blank control was also carried out simultaneously. The removal rate of S^{2-} is given as follows:

$$\eta = \frac{C_1V_1 - \left(C_2V_2 - C_3V_3/2\right)}{C_1V_1} \times 100\% ,$$

where: C_1 – S^{2-} concentration of raw water sample, 3.125×10^{-3} $mol{\cdot}L^{-1}$; V_1 – Volume of water sample to be tested, 100 mL; C_2 – Concentration of iodine standard solution, 5×10^{-3} $mol{\cdot}L^{-1}$; V_2 – Dosage of iodine standard solution (mL); C_3 – Concentration of sodium thiosulfate standard solution, 5×10^{-3} $mol{\cdot}L^{-1}$; V_3 – Dosage of sodium thiosulfate standard solution (mL).

2. Results and discussion

2.1. Preparation of FeOOH and FeOOH@ZnO and their adsorption performance toward S^{2-}

2.1.1. Adsorption performance of S^{2-} on FeOOH prepared by adding SDS at different hydrothermal temperatures

Temperature is an important regulation parameter of hydrothermal reaction, which directly affects the growth process of the material, resulting in changes in the morphology and properties of the product. The addition of surfactant can also inhibit the growth of crystal face and control the morphology of the product. Herein, the concentration of $FeCl_3$ and NaOH solution was fixed at 1.0 mol, and the hydrothermal reaction time was 8 h. The hydrothermal reaction temperature and the added amount of SDS were changed to prepare multiple groups of FeOOH. The performance toward adsorption of S^{2-} is presented in Figure 1.

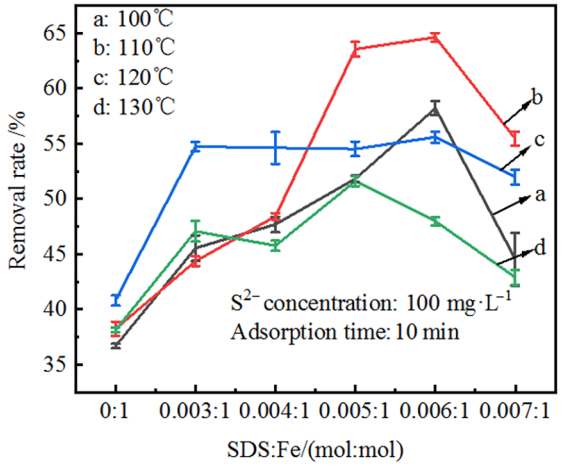

Figure 1. Adsorption performance of FeOOH toward S^{2-}, prepared by adding SDS at different hydrothermal temperatures

Figure 1 exhibits four broken lines a, b, c, and d, indicating that at different hydrothermal temperatures, the adsorption performance of FeOOH prepared with SDS is better than that of FeOOH prepared without SDS (SDS:Fe = 0:1). Moreover, with the increase of the added amount of SDS, the adsorption performance of FeOOH prepared at different hydrothermal temperatures first exhibited the strengthening effect followed by the weakening effect. When the molar ratio of SDS:Fe is 0.006:1, at the hydrothermal temperature of 110 °C (see Figure 1b), the prepared sample exhibits the best adsorption performance for S^{2-}. Analysis shows that SDS mainly plays a role of dispersion in FeOOH preparation. When the concentration is low, part of the crystal surface gets covered with SDS, which inhibits the crystal growth, reduces the particle size, and increases the SSA of the material, which is conducive to the adsorption of S^{2-}. In contrast, when the SDS concentration is high, the SDS adsorbed on the FeOOH precipitates during the hydrothermal process and is not easy to clean. Moreover, a small amount of residues appear in the final FeOOH sample, leading to the shielding of the active points of material and decrease in the ability to adsorb S^{2-}. Further analysis indicated that when the SDS:Fe molar ratio was 0.006:1 and the hydrothermal reaction temperature was 100 and 110 °C (Figures 1a and 1b), respectively, the prepared FeOOH exhibited better adsorption performance toward S^{2-} than FeOOH prepared at 120 and 130 °C (Figures 1c and 1d). This result is attributed to the fact that FeOOH is metastable material. If the temperature is too high, it gets directly decomposed into Fe_2O_3. In general, the SSA of Fe_2O_3 is smaller than

that of FeOOH, which is not conducive to the adsorption of S^{2-}. Therefore, it was finally determined that the optimized hydrothermal reaction temperature was 110 °C, and the molar ratio of SDS:Fe was 0.006:1. The adsorption and removal rate of S^{2-} by FeOOH prepared under this condition could reach 64.6%.

2.1.2. Adsorption of S^{2-} by zinc-doped FeOOH

Zinc oxide is a type of fine desulfurizer. It is widely used in raw material purification in industrial production and has high sulfur capacity (Wu et al., 2018). However, it is rarely used in wastewater treatment. In order to further improve the adsorption of S^{2-} by FeOOH, herein, under the conditions of hydrothermal temperature of 110 °C, S^{2-} concentration of 100 mg·L^{-1}, hydrothermal time of 8 h, and SDS:Fe molar ratio of 0.006:1, Zn^{2+} and ZnO were used as the doping forms of zinc to investigate the adsorption performance of zinc element-doped FeOOH (FeOOH@ZnO), and the results are shown in Figure 2. The figure illustrates that after adding equal amounts of nano-ZnO and Zn^{2+}, respectively, the adsorption effect of FeOOH containing directly doped ZnO is better than that produced by Zn^{2+} doping. The analysis indicates that when Zn element is doped into FeOOH in ionic form, Zn is mainly present as $Zn(OH)_2$ because it has not been roasted at high temperature. However, $Zn(OH)_2$ does not have good desulfurization effect and covers the adsorption activity sites of FeOOH, thus complexing with FeOOH does not offer synergistic effect on the adsorption of S^{2-}. In contrast, owing to the good dispersibility of ZnO under the action of anionic surfactant (Pang et al., 2009), incorporated nano ZnO acts as crystal nucleus to promote the formation of iron precipitates. Moreover, the precipitate formed under hydrothermal conditions gets redissolved-crystallized to form FeOOH-encapsulated ZnO complex. Both ZnO and FeOOH can adsorb S^{2-}; therefore, the performance of FeOOH doped with nano-ZnO (FeOOH@ZnO) is significantly better than that of FeOOH without ZnO. Figure 2 demonstrates that when the molar ratio of Fe:Zn is 4.0:1, the removal rate of S^{2-} by FeOOH can reach up to 71.8%. Too high or low doping amount of nano ZnO leads to the decrease in the adsorption performance of FeOOH; however, the fluctuation range is not large. This is attributed to the fact that when the doping amount of ZnO is too low, it has little effect on the adsorption performance of S^{2-}, resulting in no significant improvement in the adsorption effect. When the doping amount of ZnO is too high, the dispersibility becomes poor and multiple ZnO particles aggregate to form large particles of FeOOH@ZnO. Reduction in the SSA results in the decrease in the effect of removing sulfur ions, thus the doping amount needs to be controlled.

2.1.3. Adsorption of S^{2-} on FeOOH@ZnO prepared by changing the concentration of crystalline ions

During the hydrothermal reaction, if the concentration of crystalline ions is too high, smaller particles are easily formed and the product structure is unstable. In contrast, if the concentration is too low, the precipitated crystal particles become larger, reducing the SSA of the product, which is not conducive to the adsorption. Therefore, in this section, preparation of FeOOH@ZnO by changing the crystalline ion concentration is presented and its S^{2-} adsorption performance is discussed. Figure 3 exhibits the test results, revealing that when the ion concentration increases from 0.4 to 1.0 mol·L^{-1}, the adsorption performance of the prepared FeOOH@ZnO shows an upward trend. When the crystalline ion concentration is 1.0 mol·L^{-1}, FeOOH@ZnO exhibits the best adsorption performance for S^{2-}, and the removal rate of S^{2-} in water is the best, up to 72.1%. With the further increase of ion concentration, the adsorption performance and removal of S^{2-} begins to decrease. When the crystalline ion concentration is 1.25 mol·L^{-1}, the removal rate of S^{2-} is 63.6%, and when the crystalline ion concentration reaches 1.5 mol·L^{-1}, it further drops to 54.2%. Analysis shows that if the concentration of crystalline ions is too high, although numerous smaller particles are generated, the probability of smaller particles colliding to form larger particles increases, resulting in a decrease in the SSA of the aggregated material and affecting the adsorption and removal performance toward S^{2-} present in water.

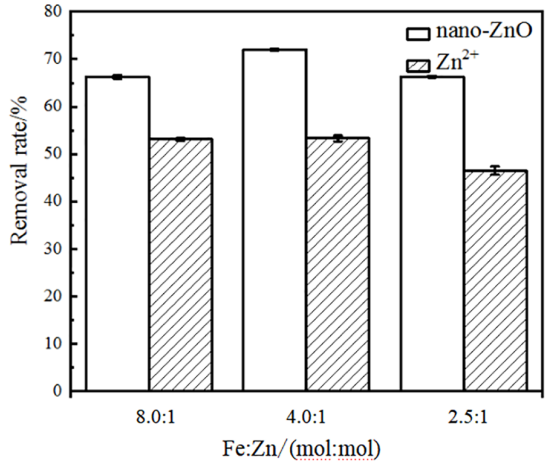

Figure 2. Adsorption of S^{2-} by zinc-doped FeOOH

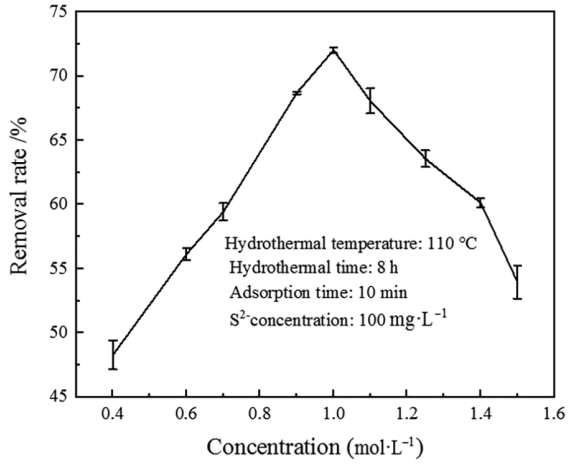

Figure 3. Adsorption of S^{2-}on FeOOH@ZnO prepared by changing the concentration of crystalline ions

2.2. FeOOH@ZnO adsorption time curve

2.2.1. The effect of adsorption time on the adsorption performance of FeOOH@ZnO for S^{2-}

The S^{2-} adsorption time curve of prepared FeOOH@ZnO is shown in Figure 4. The figure illustrates that the removal rate is the most obvious at 10 min before adsorption, and the adsorption removal rate of FeOOH@ZnO toward S^{2-} is 71.8%. With the extension of time, the removal rate increased linearly, but the increase rate decreased. When the adsorption time reached 60 min, the adsorption removal rate of S^{2-} reached 90.0%. With the further extension of the adsorption time, the removal rate also decreased slightly; however, the change was not significant. It indicates the occurrence of physical adsorption process during the adsorption of S^{2-}. With the further extension of the adsorption stirring time, a small amount of the adsorbed S^{2-} gets desorbed, resulting in slight decrease in the adsorption effect. In summary, the adsorption amount of FeOOH@ZnO reached saturation when it was adsorbed for 60 min, thus the optimized adsorption time was determined to be around 60 min. At this time, the S^{2-} adsorption removal rate was 87.5%, and the adsorption capacity was 87.5 $mg \cdot g^{-1}$. Under the same adsorption conditions, the adsorption performance of FeOOH@ZnO for S^{2-} is better than that of fermented rice husk (Xie et al., 2015).

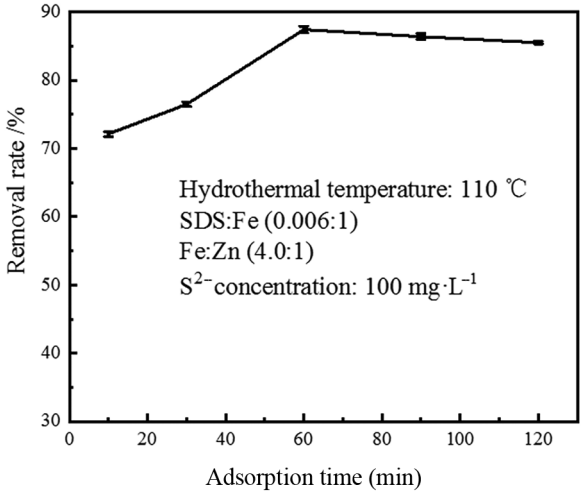

Figure 4. FeOOH@ZnO adsorption time curve

2.2.2. Effect of S^{2-} concentration on the adsorption performance of FeOOH@ZnO

The adsorption performance curve of FeOOH@ZnO for different concentrations of S^{2-} (50, 75, 100, 125, and 150 $mg \cdot L^{-1}$) is shown in Figure 5. When the adsorption test was performed, the pH of the solution containing different concentrations of S^{2-} was also measured. The results are shown in Figure 5.

Figure 5 illustrates that with the increase of the initial concentration of S^{2-}, the pH of the solution increases; however, the adsorption and removal rate of S^{2-} by FeOOH@ZnO decrease significantly. When the initial concentration of S^{2-} is 50 $mg \cdot L^{-1}$, the pH is 7.5 and the maximum S^{2-} removal rate is 99.5%. When the initial concentration of S^{2-} increases to 150 $mg \cdot L^{-1}$, the pH is 8.5, and the S^{2-} adsorption removal rate is only 75.9%. Analysis indicates that when the initial concentration of S^{2-} is low, the pH of the solution is also relatively low. FeOOH@ZnO has a tendency to dissociate metal ion, S^{2-} can react with a small amount of ions in the solution, and can also be deposited on the surface or inside of FeOOH@ZnO, thus almost all S^{2-} ions in the solution can be adsorbed and removed. When the initial concentration of S^{2-} is large, the pH of the solution increases, and the tendency of FeOOH@ZnO to dissociate ions gets weakened. S^{2-} is continuously deposited on the surface of FeOOH@ZnO, occupying the adsorption site to generate products, which block the pores. As a result, the active sites inside FeOOH@ZnO cannot be fully utilized, leading to the decrease in the S^{2-} removal rate.

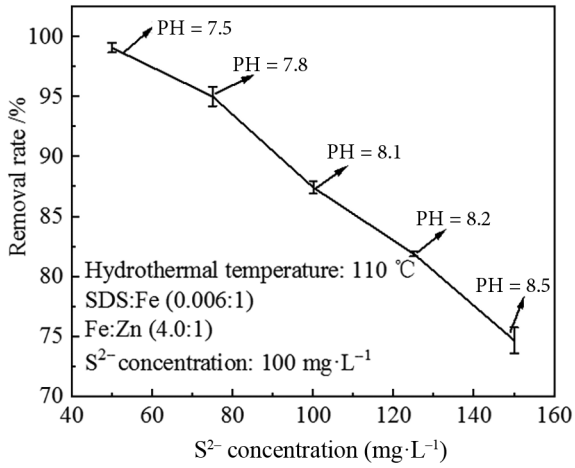

Figure 5. Effect of S^{2-} concentration on the adsorption performance of FeOOH@ZnO

2.3. Characterization

2.3.1. XRD analysis

Figure 6 shows XRD patterns of FeOOH, SDS-modified FeOOH, and FeOOH@ZnO samples. Figure 6a shows that diffraction peaks appear at 2θ values of 21.2°, 33.15°, 36.3°, and 53.2°. Compared to the standard spectrum, they correspond to the diffraction peaks of the (110), (130), (101), and (221) crystal faces of α-FeOOH, indicating that the prepared material is α-FeOOH. When SDS was added during the preparation (see Figure 6b), diffraction peaks with weaker (310) and (211) crystal planes appeared at 2θ 26.8° and 35.3°, while other strong diffraction peaks disappeared. This is attributed to the fact that SDS is adsorbed on the crystal face of α-FeOOH after its addition, thus inhibiting the formation of some crystal faces of α-FeOOH, forming β-FeOOH. However, the peak of β-FeOOH is weak, thus the crystallinity of this sample is poor. XRD patterns (see Figure 6c) of FeOOH after adding nano-zinc oxide also show weak diffraction peaks at 26.8°

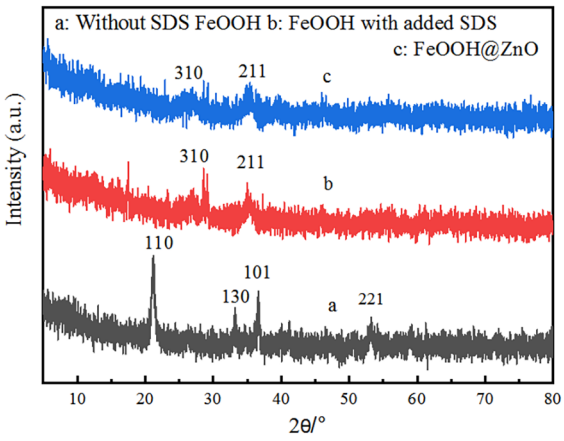

Figure 6. XRD patterns

and 35.3° corresponding to (310) and (211) planes. The diffraction peaks of nano-ZnO and some composites are not observed. It shows that the material also mainly exists in the form of β-FeOOH with poor crystallinity, and nano-ZnO is wrapped inside by FeOOH. The reason is that after adding nano-ZnO particles, ZnO can serve as crystal nucleus, causing FeOOH particles to precipitate on it and forming zinc inside and iron outside, that is, structure in which FeOOH wraps nano-ZnO.

2.3.2. SEM and TEM analysis

Figure 7 shows SEM and TEM images of FeOOH series of materials. Figure 7a illustrates that FeOOH particles exhibit nanorod-like shape, and the diameter of the rods is about 30 to 50 nm with varying length. However, the rod-like structure of FeOOH (Figure 7b) after SDS treatment disappears, and layered structure is formed by the accumulation of numerous small particles. After adding nano-ZnO (Figure 7c), the surface roughness of the material increases, numerous small particles gather together, and the boundaries between the particles are obvious. The SSA test showed that the SSA of FeOOH before and after SDS treatment was 72.5 and 112.7 $m^2 \cdot g^{-1}$, respectively. After doping nano-ZnO, the SSA of FeOOH@ZnO increased to 191.0 $m^2 \cdot g^{-1}$, which is consistent with the effect presented in the SEM image. The larger the SSA, the more the adsorption sites are formed on the surface and the better the adsorption capacity, which is consistent with the results of S^{2-} adsorption test. Figure 7d shows TEM images of FeOOH@ZnO, illustrating that the FeOOH@ZnO particles are larger and the edges of the particles are lighter in color, but there are obvious dividing lines and the internal color is uneven. Combined with XRD analysis, it was speculated that this result was caused by the overlap of different materials of nano ZnO and FeOOH. According to the proportion of added zinc oxide and XRD test results, the outside of the large particles should be FeOOH material, and nano-ZnO should exist inside the particles. However, the size of the added nano-ZnO is about 20 nm, and the size of the formed particles is about 200 nm. The difference is large, thus the large particles should be made up of multiple irons and small particles including gently agglomerated zinc.

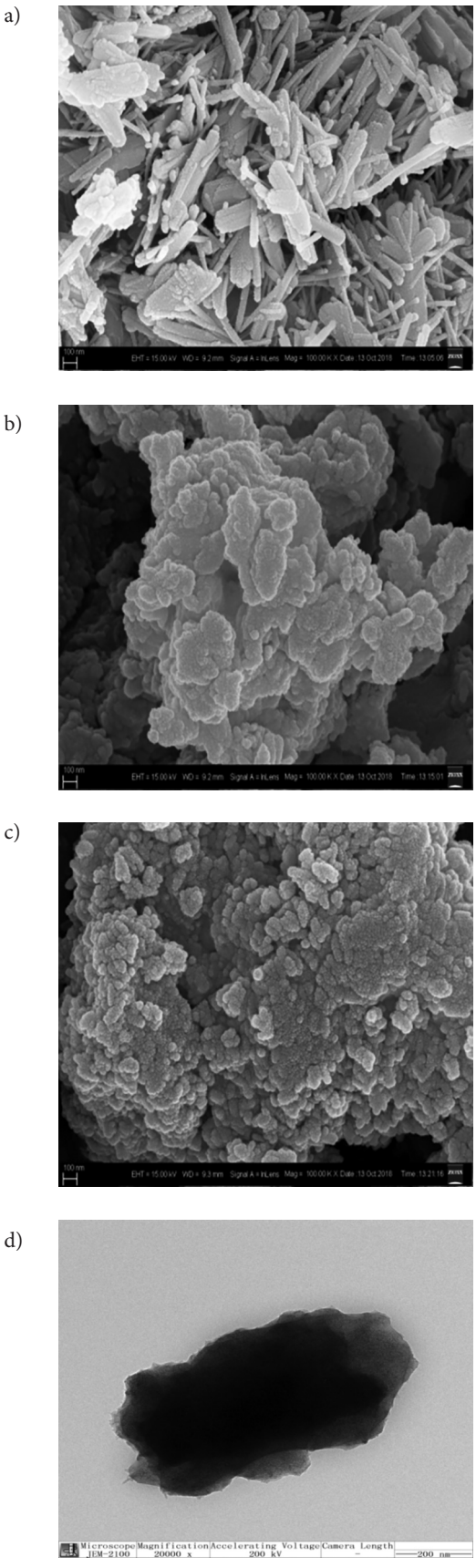

Figure 7. SEM and TEM images: a) SEM image of FeOOH sample without SDS, b) SEM image of FeOOH sample with added SDS, c) SEM image of FeOOH@ZnO, and d) TEM image of FeOOH@ZnO

2.3.3. FTIR spectroscopy and Raman analysis

In order to further analyze the chemical bond and functional group information of the material, the IR and Raman spectra of FeOOH, SDS-modified FeOOH, and FeOOH@ZnO were analyzed. The results are shown in Figure 8. Figure 8a illustrates that the absorption peak appearing at 3420 cm^{-1} is attributed to the hydroxyl vibration peak of the surface adsorbed water, and the peak appearing at about 3422 cm^{-1} is attributed to the absorption peak of OH of FeOOH. The absorption peaks at about 787 and 895 cm^{-1} belong to the vibration peak of Fe–O–H in FeOOH, and the stretching vibration peak of Fe–O appears at 601 cm^{-1}. Comparative analysis of Figures 8b and 8c indicates that absorption peaks of both the SDS-modified FeOOH and FeOOH@ZnO are red-shifted and become weaker and wider. At the same time, the characteristic peaks of SO_4^{2-} appear at 1463, 1524, and 1626 cm^{-1}, indicating that SDS adsorption affects the crystal shape of the material, which is consistent with the results of XRD and SEM analysis. It is considered that the FeOOH and FeOOH@ZnO particles become smaller after the addition of SDS, and the crystalline particles become amorphous, thus the absorption peaks of Fe–O–H and Fe–O become weak. The red shift appears to be caused by the decrease in the particle size of the sample, strengthening of the hydrogen bonds in the molecule, and increase in the stability of the structure. Figure 9a demonstrates that the peaks at 210, 415, 477, and 587 cm^{-1} are all attributed to FeOOH. Figure 9b shows Raman spectrum of the added nano ZnO, revealing that the intensity of the corresponding peaks is slightly weakened. It also indicates the interaction between FeOOH and nanoZnO. Raman diagram does not directly detect the peak of nano-ZnO, thus proving that nano-ZnO is encapsulated by FeOOH.

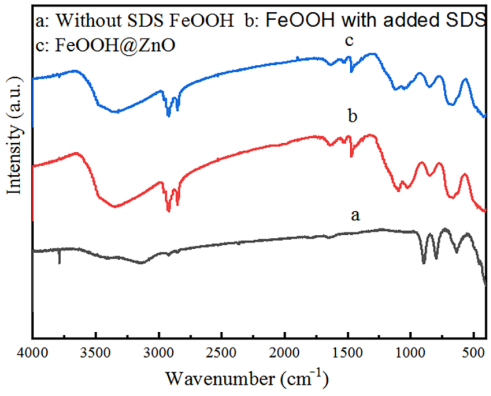

Figure 8. FTIR spectra

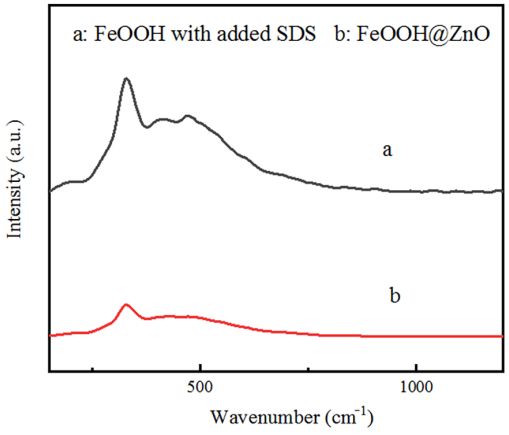

Figure 9. Raman spectra

2.3.4. Specific surface area and pore structure analysis

Figure 10 shows the nitrogen adsorption and desorption isotherms before and after adsorption of S^{2-} by FeOOH@ZnO. Figure 10a illustrates that in the low pressure zone with P/P0 in the range of 0.0–0.3, the isotherm is biased to the X axis and in the medium pressure zone with P/P0 of 0.3–0.8, it is also biased to the X axis. According to the IUPAC classification standard, it belongs to the type III isotherm adsorption line. When P/P_0 is below 0.2, the amount of N_2 adsorption is less, about 30 $mL \cdot g^{-1}$. When P/P_0 is between 0.2–0.8, the amount of N_2 adsorption is about 180 $mL \cdot g^{-1}$. For P/P0 higher than 0.8, the adsorption capacity of N_2 is about 180 $mL \cdot g^{-1}$. That is to say, the adsorption capacity increases with the increase in the partial pressure. It indicates that the FeOOH@ZnO bulk material is mainly mesoporous, and there exist a large number of large or stacked pores, and only a small number of micropores. Figure 10b exhibits that the adsorption

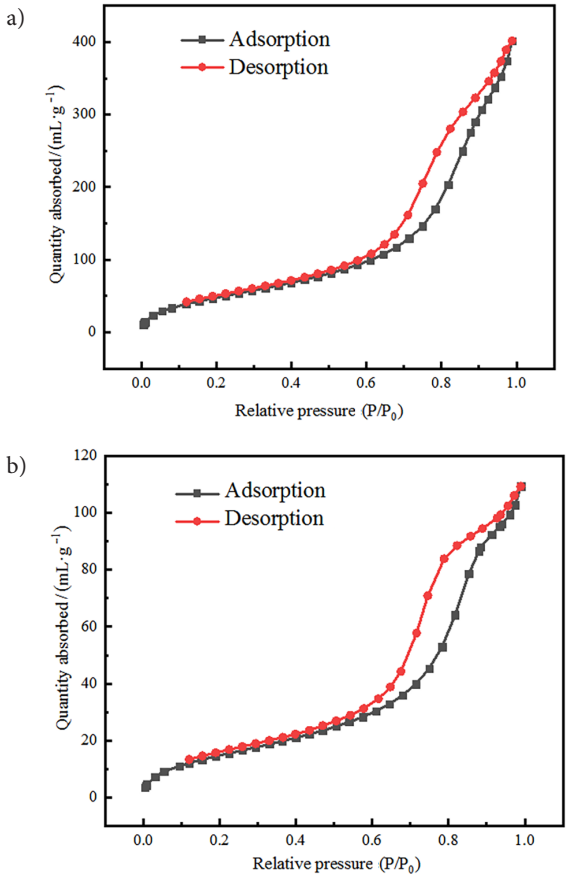

Figure 10. Nitrogen adsorption/desorption diagrams before and after adsorption by FeOOH@ZnO: a) Before adsorption and b) After adsorption

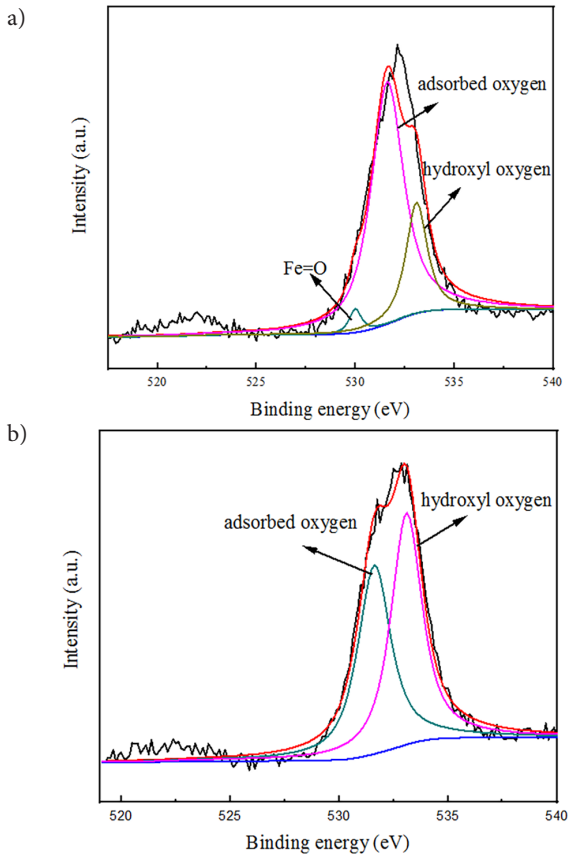

Figure 11. O_{1s} XPS fit diagrams: a) Before adsorption and b) After adsorption

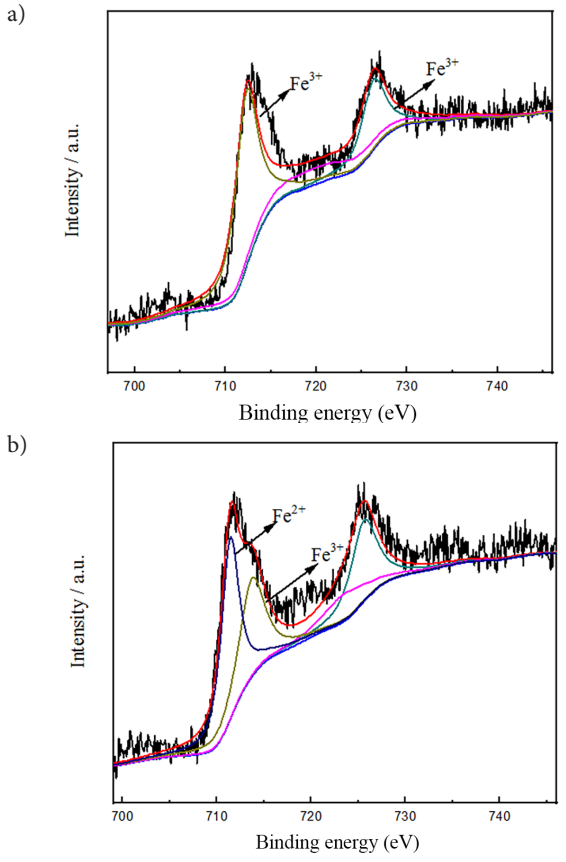

Figure 12. Fe_{2p} XPS fit diagrams: a) Before adsorption and b) After adsorption

amount is about 8 $mL \cdot g^{-1}$ in the low pressure zone with P/P_0 of 0.0–0.3, and about 35 $mL \cdot g^{-1}$ in the medium pressure zone with P/P_0 of 0.3–0.8. In the high pressure zone where P/P_0 is higher than 0.8, it is about 77 $mL \cdot g^{-1}$, and its adsorption capacity is much lower than that before adsorption. At the same time, it also showed that the products of FeOOH@ZnO adsorbed S^{2-} accumulated in the mesopores and macropores, which resulted in the decrease of pore volume and SSA.

2.3.5. XPS analysis

XPS was used to further analyze the surface chemical state of FeOOH@ZnO before and after adsorption of S^{2-}. The O_{1s} fitting results are shown in Figure 11. Figure 11a indicates that O_{1s} peaks at 530.0, 531.6, and 533.1 eV are attributed to the hydroxyl oxygen in Fe = O, adsorbed oxygen, and H_2O, respectively. After adsorption of S^{2-} (Figure 11b), O_{1s} only fitted the adsorption oxygen and H_2O, and the hydroxyl oxygen in H_2O increased. It is believed that the adsorption process follows the following reaction: $FeOOH + S^{2-} \rightarrow Fe_2S_3 \cdot H_2O + H_2O$. The oxygen in Fe = O is replaced by sulfur, and iron sulfide and water are formed.

The fitting results of Fe_{2p} are shown in Figure 12. Figure 12a illustrates that the fitting peaks at 712.6 and 726.3 eV are attributed to Fe^{3+}. After adsorption of S^{2-}, the photoelectron peaks of $Fe_{2p1/2}$ appear at high binding energy, and the fitting peaks at 711.4 and 713.0 eV are attributed to Fe^{2+} and Fe^{3+}, respectively. It is indicated that Fe^{2+} appears in the material after adsorption of S^{2-}. It is believed that $Fe_2S_3 \cdot H_2O$ gets further decomposed after it is formed, $Fe_2S_3 \rightarrow FeS + FeS_2$, and the presence of green particles in the solution also confirms the existence of ferrous precipitation.

Conclusions

Using Fe^{3+} and OH^- as crystal ions, FeOOH crystal material was prepared by hydrothermal method. Too high hydrothermal temperature or too low amount of added SDS was not conducive to FeOOH adsorption performance toward S^{2-}, and the adsorption of S^{2-} by nano-ZnO doped was further increased. When the hydrothermal reaction temperature was 110 °C, the adsorption time was 60 min, the SDS:Fe molar ratio was 0.006:1, the Fe:Zn molar ratio was 4.0:1, and the adsorption capacity of the prepared FeOOH@ZnO toward S^{2-} could reach 87.5 $mg \cdot g^{-1}$. If the adsorption time was too long and the initial concentration of S^{2-} in the solution was too high, the adsorption removal rate of S^{2-} decreased.

Structural analysis showed that FeOOH grain formation was inhibited and the material particles changed from rod-like to granular-like after treatment with SDS and doping with nano-ZnO, carried out during the preparation process of FeOOH. No Zn-containing compounds were detected on the surface, indicating that nano-ZnO and FeOOH formed wrapped structure with decreased

crystallinity and increased specific surface area. These factors were conducive to S^{2-} adsorption removal.

The XPS fitting results showed that before the FeOOH@ZnO adsorption reaction, oxygen was mainly present as Fe = O, adsorbed oxygen, and H_2O hydroxyl oxygen, and iron was mainly present as Fe^{3+}. However, after adsorption of S^{2-}, the lattice oxygen disappeared, and only the adsorbed oxygen and hydroxyl oxygen were fitted. It indicates that the oxygen in Fe = O was replaced with sulfur, and ferrous precipitate appeared.

Acknowledgements

This research was supported by the National Natural Science Foundation of China (No. 51608166).

References

Chen, Z., Zhang, S. H., & Zhong, L. X. (2019). Simultaneous sulfide removal, nitrogen removal and electricity generation in a coupled microbial fuel cell system. *Bioresource Technology*, *291*, 121888. https://doi.org/10.1016/j.biortech.2019.121888

Chinese Standard. (2000). *Water quality. Determination of sulfides. Iodometric method* (HJ/T60-2000). https://www.chinesestandard.net/PDF/English.aspx/HJT60-2000

Du, X., Liu, J., Chen, H., & Zhang, Z. (2018). Study on the electrochemical oxidation desulfurization behavior of model diesel on anodic alumina oxide and ceria nanotubes. *Energy Fuels*, *32*(2), 2612–2621. https://doi.org/10.1021/acs.energyfuels.7b03629

Fu, H., Wang, X., Wu, H., Yin, Y., & Chen, J. (2007). Heterogeneous uptake and oxidation of SO_2 on iron oxides. *Journal of Physical Chemistry* C, *111*(16), 6077–6085. https://doi.org/10.1021/jp070087b

Jaiswal, A., Banerjee, S., Mani, R., & Chattopadhyaya, M. C. (2013). Synthesis, characterization and application of goethite mineral as an adsorbent. *Journal of Environmental Chemical Engineering*, *1*(3), 281–289. https://doi.org/10.1016/j.jece.2013.05.007

Kwong, W. L., Lee, C. C., & Messinger, J. (2016). Transparent nanoparticulate FeOOH improves the performance of a WO_3 photoanode in a tandem water-splitting device. *Journal of Pysical Chemistry C*, *120*(20), 10941–10950. https://doi.org/10.1021/acs.jpcc.6b02432

Lee, S., Lee, T., & Kim, D. (2017). Adsorption of hydrogen sulfide from gas streams using the amorphous composite of alpha-FeOOH and activated carbon powder. *Industrial & Engineering Chemistry Research*, *56*(11), 3116–3122. https://doi.org/10.1021/acs.iecr.6b04747

Liang, S. J., Mi, J. X., Liu, F. J., Zheng, Y., Xiao, Y. H., Cao, Y. N., & Jiang, L. L. (2020). Efficient catalytic elimination of COS and H_2S by developing ordered mesoporous carbons with versatile base N sites via a calcination induced self-assembly route. *Chemical Engineering Science*, *221*, 115714. https://doi.org/10.1016/j.ces.2020.115714

Liu, C., Yuan, P., Duan, A. J., Mei, J. L., Zheng, P., Meng, Q., Cai, A. F., Cheng, T. T., & Gong, Y. J. (2019). Monodispersed dendritic mesoporous silica/carbon nanospheres with enhanced active site accessibility for selective adsorptive desulfurization. *Journal of Materials Science*, *54*(11), 8148–8162. https://doi.org/10.1007/s10853-019-03461-4

Liu, X., Qiu, G., Yan, A., Wang, Z., & Li, X. (2007). Hydrothermal synthesis and characterization of alpha-FeOOH and alpha-Fe_2O_3 uniform nanocrystallines. *Journal of Alloysand Compounds*, *433*(1–2), 216–220. https://doi.org/10.1016/j.jallcom.2006.06.029

Liu, X. L., Pang, H. W., Liu, X. W., Li, Q., Zhang, N., Mao, L., Qiu, M., Hu, B., Yang, H., & Wang, X. (2021). Orderly porous covalent organic frameworks-based materials: Superior adsorbents for pollutants removal from aqueous solutions. *The Innovation*, *2*(1), 100076. https://doi.org/10.1016/j.xinn.2021.100076

Liu, Y., Song, C. Y., Wang, Y. C., Cao, W. H., Lei, Y. P., Feng, Q. G., Chen, Z., Liang, S. J., Xu, L., & Jiang, L. L. (2020). Rational designed Co@N-doped carbon catalyst for high-efficient H_2S selective oxidation by regulating electronic structures. *Chemical Engineering Journal*, *401*, 126038. https://doi.org/10.1016/j.cej.2020.126038

Pang, J. S., Zhang, H. Y., & Cao, B. (2009). Research on dispersion of ZnO nanoparticles in aqueous coating system. *Bulletin of the Chinese Ceramic Society*, *28*(1), 108–112+116.

Qian, J., Zhou, J. M., Pei, X. J., Zhang, M. K., & Liu, Y. (2019). Bioactivities and formation/utilization of soluble microbial products (SMP) in the biological sulfate reduction under different conditions. *Chemosphere*, *221*, 37–44. https://doi.org/10.1016/j.chemosphere.2018.12.208

Seabold, J. A., & Choi, K. S. (2012). Efficient and stable photooxidation of water by a bismuth vanadate photoanode coupled with an Iron oxyhydroxide oxygen evolution catalyst. *Journal of the American Chemical Society*, *134*(4), 2186–2192. https://doi.org/10.1021/ja209001d

Song, H. J., Xia, L. X., Jia, X. H., & Yang, W. M. (2018). Polyhedral alpha-Fe_2O_3 crystals@RGO nanocomposites: Synthesis, characterization, and application in gas sensing. *Journal of Alloys and Compounds*, *732*, 191–200. https://doi.org/10.1016/j.jallcom.2017.10.205

Tang, X. D., Jiao, S., Li, J. J., & Hu, N. (2018). Deep desulfurization of kerosene by electrochemical oxidation and extraction in Mn^{2+}/Mn^{3+} electrolyte. *Petroleum Science and Technology*, *36*(7), 500–506. https://doi.org/10.1080/10916466.2018.1428624

Wei, S. L. (2003). Environmental pollution and treatment method of sulfides in tannery effluents. *China Leather*, *32*(1), 3–5.

Wu, M. M., Shi, L., Lim, T. T., Veksha, A., Yu, F., Fan, H. L., & Mi, J. (2018). Ordered mesoporous Zn-based supported sorbent synthesized by a new method for high-efficiency desulfurization of hot coal gas. *Chemical Engineering Journal*, *353*, 273–287. https://doi.org/10.1016/j.cej.2018.07.134

Xiao, F., Li, W. T., Fang, L. P., & Wang, D. S. (2016). Synthesis of akageneite (beta-FeOOH)/reduced graphene oxide nanocomposites for oxidative decomposition of 2-chlorophenol by Fenton-like reaction. *Journal of Hazardous Materials*, *308*, 11–20. https://doi.org/10.1016/j.jhazmat.2016.01.011

Xie, X. M., Liao, M., Hua, J. Y., Chen, N., Zhang, N., Xu, P. Z., Xie, K. Z., Xu, C. X., & Liu, G. R. (2015). Adsorption-desorption characteristics of fermented rice husk for ferrous and sulfur ions. *Environmental Science*, *36*(10), 3896–3905.

Yang, T. T., Meng, L. R., Han, S. W., Hou, J. H., Wang, S. S., & Wang, X. Z. (2017). Simultaneous reductive and sorptive removal of Cr(VI) by activated carbon supported beta-FeOOH. *RSC Advances*, *7*(55), 34687–34693. https://doi.org/10.1039/C7RA06440C

Zhang, S. W., Gao, H. H., Huang, Y. S., Wang, X. X., Hayat, T., Li, J. X., Xu, X. J., & Wang, X. K. (2018a). Ultrathin g-C_3N_4 nanosheets coupled with amorphous Cu-doped FeOOH

nanoclusters as 2D/0D heterogeneous catalysts for water remediation. *Environmental Science: Nano*, *5*(5), 1179–1190. https://doi.org/10.1039/C8EN00124C

Zhang, Y. P., Zhang, L., Li, L. H., Chen, G. H., & Jiang, F. (2018b). A novel elemental sulfur reduction and sulfide oxidation integrated process for wastewater treatment and sulfur recycling. *Chemical Engineering Journal*, *342*, 438–445. https://doi.org/10.1016/j.cej.2018.02.105

Zhou, L., Liu, Y., Luo, L. Y., Yuan, Z. L., Yang, L. J., & Wu, H. J. (2019). Improving the removal of fine particles by chemical agglomeration during the limestone-gypsum wet flue gas desulfurization process. *Journal of Environmental Sciences*, *80*, 35–44. https://doi.org/10.1016/j.jes.2018.07.013